



# Cloud microphysical profile differences pertinent to monsoon phases: inferences from a cloud radar

Patra Sukanya<sup>1,2</sup> · M. C. R. Kalapureddy<sup>1,2</sup>

Received: 9 July 2018 / Accepted: 4 March 2019 / Published online: 18 March 2019  
© Springer-Verlag GmbH Austria, part of Springer Nature 2019

## Abstract

Microphysical evolution of tropical clouds in the core monsoon region of India is examined for the first time using ground-based cloud radar measurements. Combining high-resolution radar reflectivity ( $Z$ ) profiles with empirical relations, cloud microphysical profiles in terms of cloud ice/liquid water content (IWC/LWC) during Indian summer monsoon (ISM) season are retrieved. Though the study is carried out using a point observation, it is shown that it represents the large-scale monsoon flow over the radar site. Cloud radar measurements during ISM period are classified into active and break ISM days. Radar-derived IWC profiles are validated against CloudSat, whereas LWC profiles are validated using the collocated microwave radiometer and microphysical observations from in situ aircraft measurements. The validated IWC and LWC profiles show significant differences between active and break ISM phases including their diurnal evolution. Larger (smaller) IWC values observed during active (break) days reveal the microphysical activity associated with the contrasting cloud vertical structure in the respective ISM phases. Observed discontinuity in the cloud vertical structure during break ISM days is attributed to the lack of moist convection. The significance of the present study lies in reporting the first ground-based radar measurements of cloud microphysical properties during active and break ISM period and discussing their distinctiveness.

## 1 Introduction

Clouds play a crucial role in climate change and the general circulation of the atmosphere through radiative transfer and precipitation. These radiative properties and precipitation efficiency of clouds are determined by their several microphysical properties, for instance the liquid water content (LWC), ice water content (IWC), droplet size distribution (DSD) and the phase of cloud particles (Liou 1992; Sassen et al. 1999; Protat et al. 2007; Khain et al. 2008; Ellis and Vivekanandan 2011; Nair et al. 2012). Cloud microphysical properties are basically related to the growth or decay

of cloud water content or its change of phase. Similar to the vertical structure of atmosphere, cloud vertical structure can also be defined as the height distribution of cloud water mass with respect to changing temperature. Either for cloud-resolving simulations or radiative transfer model, detailed high-resolution (e.g., order of a few tens of meters and hour or less; Sui et al. 2005) cloud vertical structure or vertical profiles of cloud physical parameters are required to know the precipitation efficiency or radiative influence of clouds.

There are usually two distinct phases in typical Indian summer monsoon (ISM): active and break phases, which are characterized by high and low rainfall, respectively. This contrast in rainfall between these phases is one of the sources of intraseasonal variability in monsoon season of India (June–September). Active ISM phase is characterized by persistent large cloud cover, frequent rain spells, condition favorable for convective activity, large-scale low-level convergence and cloud development due to sustained rich moisture influx by the continuous strong low-level westerly wind from Arabian Sea (e.g., Kalapureddy et al. 2007). During break ISM phase, the weak low-level westerly, scant moisture influx and meager vertical velocity result in the weaker convective conditions that could be the reason for either no or only shallow convective clouds and

Responsible Editor: S.-W. Kim.

**Electronic supplementary material** The online version of this article (<https://doi.org/10.1007/s00703-019-00666-9>) contains supplementary material, which is available to authorized users.

✉ M. C. R. Kalapureddy  
kalapureddy1@gmail.com

<sup>1</sup> Indian Institute of Tropical Meteorology (IITM), Dr Homi Bhabha Road, Pashan, Pune 411008, India

<sup>2</sup> Atmospheric and Space Science Division, Savitribai Phule Pune University, Pune 411007, India

scanty rainfall implying dry conditions (Raghavan 1973). Break ISM phase is favorable for high solar insolation due to less or broken cloud cover, that leads to the formation of local isolated deep convective clouds which is the source of widely spread thin cirrus cloud that exists for longer time at high altitudes.

The active and break cycles are generally linked to the northward-propagating intraseasonal oscillation (ISO, e.g., Goswami and Ajaya Mohan 2001) and act as primary building block of ISM (e.g., Abhik et al. 2013). During the ISM period, India receives more than 70% of its annual rainfall. Therefore, ISM performance has profound implication directly for the agriculture production and thus the socio-economic growth of India. Further, contrasting behaviors in the formation of weather systems and large-scale instability during active and break ISM periods are well established (e.g., Goswami et al. 2003; Ravikiran et al. 2009; Devasthale and Grassl 2009). Earlier studies on the ISM phases were mostly confined to rainfall, circulation pattern and mesoscale convection (Webster et al. 1998; Goswami and Ajaya Mohan 2001; Gadgil 2003; Rajeevan et al. 2010). Due to the lack of cloud measurements with better spatial and temporal resolutions during ISM spells, some of the previous studies realized the importance of cloud vertical structure but are unable to utilize it for better accountability of monsoon rainfall variability. It is now possible to access the global cloud vertical structure information from the space-borne cloud profiling radar (CPR) with the CloudSat. Renewed interest on cloud vertical structure using CPR measurements confining to ISM region has been found in the recent studies (Das et al. 2013; Rajeevan et al. 2013). Therefore, it is now established that high-resolution vertical profile of cloud microphysics is a key parameter in understanding the dynamical and physical mechanisms of clouds pertinent to active and break spells of ISM rainfall (Konwar et al. 2014; Hazra et al. 2017).

Still, due to the absence of continuous high temporal resolution cloud observations, a complete understanding of diurnal evolution of clouds and their role in driving the mean monsoon circulation is lacking. This gap can be bridged now by using ground-based cloud radar measurements, which have a much better resolution with respect to both space and time compared to direct aircraft- or balloon-based cloud sampling techniques (Matrosov 1997; Kollias et al. 2007). Recently, radars have been recognized for their potential to quantitatively measure the microphysical properties of clouds (Matrosov 1997; Das et al. 2013; Rajeevan et al. 2013). Both cloud microphysics and dynamics influence structural evolution of ISM clouds that is further related to rainfall (Sengupta et al. 2013). So the estimation of IWC or LWC profiles is helpful to understand the underlying cloud microphysical processes involved in the formation and maintenance of ISM cloud systems. These profiles also assist the representation

of clouds in numerical and general circulation models. In recent times, one of the largest errors in weather and climate models is attributed to the lack of knowledge of the interaction between cloud microphysics and the environment.

A number of procedures have been developed recently to estimate the microphysical features of clouds from millimeter-wavelength radar observations (Frisch et al. 2000). Sassen and Liao (1996) and Khain et al. (2008) employed a numerical cloud model to obtain a useful relationship between radar reflectivity and LWC. Attempts have been made to find the relationships between radar reflectivity and LWC for stratocumulus and cumulus clouds (Atlas 1954; Sauvageot and Omar 1987; Fox and Illingworth 1997). Frisch et al. (1995) developed radar–radiometer technique for retrieving microphysical features of liquid–water clouds, such as stratus. In contrast to long-wavelength radar signals, short-wavelength radar signals are attenuated by cloud liquid water. Leveraging this fact, spatial distribution of cloud liquid water can be estimated using dual-wavelength radar (Vivekanandan et al. 1999, 2001; Gaussiat et al. 2003; Hogan et al. 2005; Ellis and Vivekanandan 2011). Gossard et al. (1997) used the full spectrum of the radar-measured Doppler vertical velocities in estimating LWC. With estimating LWC, a number of attempts have been made to retrieve ice cloud in recent years, using reflectivity alone (Sassen 2002; Heymsfield et al. 2005; Sayres et al. 2008) and adding temperature as an additional constraint (Liu and Illingworth 2000; Hogan et al. 2006). Many of these studies prescribed direct reflectivity–ice water content relations, usually in the form of an empirical power-law relation, allowing the use of reflectivity values to estimate the ice water content accurately (Matrosov 1997, 1999; Mace et al. 1998; Intrieri et al. 1993; Donovan and Lammeren 2001; Donovan et al. 2001; Wang and Sassen 2001; Tinel et al. 2005; Sekelsky et al. 1999; Gaussiat et al. 2003).

The key objective of the current work is to decipher the cloud microphysical process pertinent to ISM active and break ISM phases. This study of the cloud microphysical processes is carried out by contrasting the vertical distribution of cloud water content in active and break phases. Section 2 briefly describes the cloud radar system, data and methodologies followed in this work. Results and discussions are provided in Sect. 3, which starts with the retrieval of IWC and LWC profiles using ground-based cloud radar and comparison of IWC profiles with CloudSat CPR observations. That section further discusses the radar-derived LWC profiles along with those derived using the aircraft and microwave radiometer (MWR) observations over Mandhardev region. Diurnal evolution of microphysical profiles in active and break ISM phases is covered at the end of this section. Summary of the work and the concluding remarks are provided in Sect. 4.

## 2 System, data and methodology

This study uses reflectivity profiles of vertically pointing Indian Institute of Tropical Meteorology’s Ka-band scanning polarimetric radar (KaSPR) operating at 35 GHz. KaSPR has been providing high-resolution (25 m and 1 s.) measurements of cloud and precipitation over Mandhardev (18.04°N, 73.87°E, ~1.3 km AMSL) in Western Ghats region on a mobile platform since June 2013. KaSPR operates under a hybrid scan strategy (cyclic volume scan, Range Height Indicator scan and vertical looking) to study 3-D cloud structures, and vertical pointing observations for 5 min for every 15 min are available. KaSPR possesses sensitivity of ~ -45 dBZ at 5 km and is therefore sensitive to the cloud droplet. Cloud radar, especially 35 GHz, is not only sensitive to hydrometeors (cloud particles and raindrops) but also to airborne biological targets called biota. In order to segregate the biota contribution from the radar reflectivity ( $Z$ ) measurements, an indigenously developed algorithm (TEST, Kalapureddy et al. 2018) is used to filter the KaSPR data. In brief, the TEST algorithm uses theoretical noise equivalent curves (Fig. 1a) to filter out receiver noise floor. Based on a four-point running average and standard deviation of  $Z$  at each height level, it is able to distinguish biota and cloud droplet depending on their small and long correlation period (i.e., larger and smaller standard deviation), respectively. Height–time–intensity (HTI) map of  $Z$ , depicted in Fig. 1b, shows isolated point targets mostly confined below 3.2 km, which can be mistaken as low-level clouds. Figure 1c shows the potential of the TEST algorithm in screening out only the pure meteorological liquid bodies as cloud reflectivity seen at ~3.2 to 4.4 km. Therefore, to confirm the usage of pure cloud information and unbiased study of cloud water

content, cloud measurements screened out by the TEST algorithm are only used.

The main purpose of the study is to estimate the vertical profiles of IWC and LWC. Similar to traditional power law relation between radar reflectivity factor and rainfall rate, relation between  $Z$  and the required parameter is used. Protat et al. (2007) experimented over tropical and midlatitude regions using a large statistical microphysical database from cloud radar, lidar and aircraft observations for accurate retrieval of IWC. Their works assessed the statistical significance of the IWC– $Z$  and IWC– $Z$ – $T$  relationships. These two relations as given below are used here

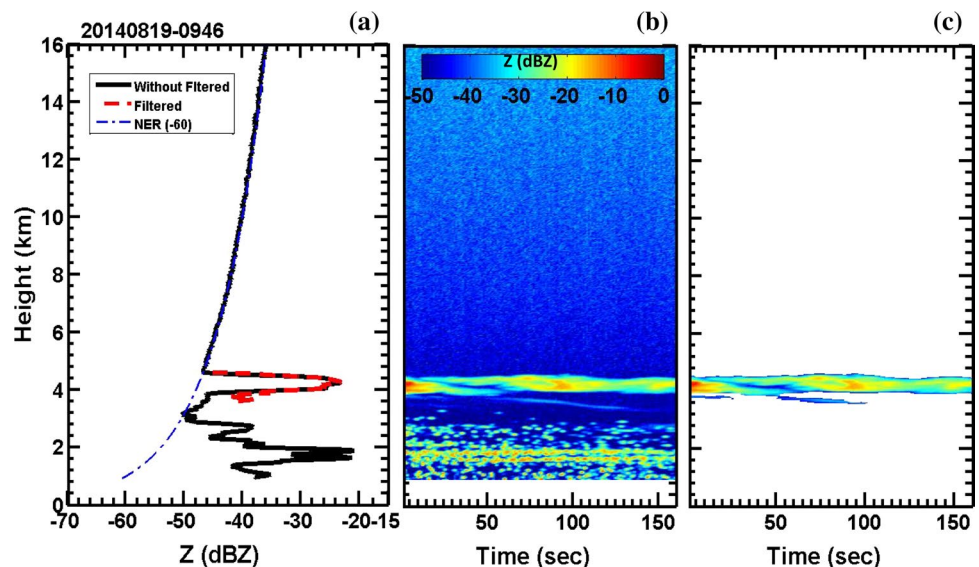
$$IWC = 0.103 * Z^{(0.6)} \tag{1}$$

$$\log(IWC) = 0.000185 * z * T + 0.0735 * z - 0.0091 * T - 1.31 \tag{2}$$

where IWC unit is  $gm\ m^{-3}$ .  $Z$  and  $z$  are the reflectivity factors in  $mm^6\ m^{-3}$  and dBZ, respectively.  $T$  is temperature in K. For LWC estimation, in general, three different radar remote sensing retrieval methods are possible. These entail using (1) empirical relation between  $Z$  and LWC, (2)  $Z$  and liquid water path (LWP) from the observations of multi-wavelength microwave radiometer (MWR) and (3)  $Z$  and cloud droplet number concentration and diameter. This paper uses the above-mentioned first two methods.

In case of empirically estimated LWC, three radar-based  $Z$ –LWC relations are adopted in this work depending on precipitation condition. Note that there is no consistent (i.e., applied to all types of clouds or to the entire  $Z$  range; irrespective of non-precipitating or drizzle cloud) relationship between  $Z$  and LWC due to the different size distributions and physical mechanisms (Khain et al. 2008). This is the main reason for no single empirical relation capable

**Fig. 1** a Vertical-looking cloud radar-measured reflectivity mean height profile on August 19 2014 during 0946–0948 UTC. The theoretical noise equivalent reflectivity (NER) curve with the respective threshold values of -60 dBZ is shown in the bracket. HTI plot of b the reflectivity profile for the duration of 180 s. c TEST screened out pure cloud reflectivity profile by filtering out the receiver noise floor and the biota (mean of the screened cloud reflectivity profile can be seen in panel a with dashed red line)



of estimating LWC irrespective of changing precipitation conditions. A detailed discussion has been made to find out reflectivity values and range of different rain rates. Earlier studies show that a threshold reflectivity value in the range  $-20$  to  $-18$  dBZ indicates a non-precipitating cloud, whereas values in the range of  $-15$  to  $-16$  dBZ are the minimum values of  $Z$  required for drizzling (Sauva-geot and Omar 1987; Frisch et al. 1995; Mace and Sassen 2000; Baedi et al. 2002). Depending on the geographical location, the threshold value deviates in the range of 1–2 dBZ. Various case studies are performed to investigate this threshold value over the present location of interest. For this purpose, besides KaSPR's  $Z$  measurements corresponding to its first range bin ( $\sim 1$  km) height above the surface, the ground-based rainfall measurements from rain gauge are also employed to categorize precipitation events into non-precipitating ( $< \sim -10$  dBZ and  $0 \text{ mm h}^{-1}$ ), light drizzling ( $-10$  to  $10$  dBZ and  $< 1 \text{ mm h}^{-1}$ ) and heavy drizzling ( $> 10$  dBZ and  $1\text{--}5 \text{ mm h}^{-1}$ ).

For non-precipitating or no rain cases, the relationship in Atlas (1954), which is based on different drop size distributions, is used where simple  $Z$  measurements of KaSPR are utilized to estimate LWC.

$$\text{LWC} = \sqrt{Z/0.048} \quad (3)$$

Retrieval of LWC for light drizzling with stratocumulus cloud is adopted from Baedi et al. (2000) that used  $Z$  and LWC from aircraft observations (FSSP and 2D cloud probe) to find out the relationship between these two parameters with constrained threshold values of  $Z$  and LWC as  $-35$  dBZ and  $0.01 \text{ gm m}^{-3}$ , respectively.

$$\text{LWC} = (Z/57.54)^{(1/5.17)} \quad (4)$$

For heavy drizzling, the relationship in Krasnov and Russchenberg (2002) is employed for estimating the LWC by using a new trajectory ensemble model of the cloud-topped boundary layer.

$$\text{LWC} = (Z/323.59)^{(1/1.58)} \quad (5)$$

In Eqs. (3), (4) and (5),  $Z$  is in  $\text{mm}^6 \text{ m}^{-3}$  and LWC is in  $\text{gm m}^{-3}$ . These three relationships for  $Z$ –LWC used here are not continuous (see Fig. A3).

Temperature profiles from radiosonde over the radar site or the presence of bright band from reflectivity shows  $0^\circ \text{C}$  isotherms around 4.5 km AMSL. So, the presence of ice particles within clouds can be predicted above this altitude. For IWC, profiles above 5 km altitude are considered, whereas for LWC, profiles below 4 km altitude (for non-precipitating cloud) are considered. But for light and heavy drizzling, since the liquid water contribution can come from the supercooled liquid droplets as well which exist above zero-degree isotherm, altitude profiles up to  $\sim 8$  km are considered.

IMD-declared monsoon spells are mostly suitable for central India region but according to Rajeevan et al. (2010; its Figs. 4 and 7) and Pai et al. (2016; its Figs. 5 and 7), it can be seen that the west coast region of India also shares near-similar mean monsoon seasonal as well as active and break ISM features with that of central India. In this context, point radar measurements around the Western Ghats region essentially can be considered as sample of large-scale spread of ISM that is mainly confined to the central and west coast part of India. The IWC/LWC composite diurnal evolution and comparison cases of profiles of IWC with CPR observation chosen in this work are also closely linked to the ISM phases. For this purpose, the core ISM active and break spells are chosen according to the Indian Meteorological Department (IMD) (monsoon report 2014; monsoon report 2015; monsoon report 2016 at [www.imd.gov.in/section/nhac/](http://www.imd.gov.in/section/nhac/)). The identification of ISM active and break spells are based on Rajeevan et al. (2010) and a Pai et al. (2016) criterion that uses daily area weighted rainfall and its long term (1951–2000) average. Whichever days exceed (deficit) the rainfall climatology mean by  $\pm 1\sigma$  (standard deviation) define it as active (break) days.

Active (July 14–16; August 3–5; and August 25–31) and break (July 3–5; August 8–10; and August 12–17) ISM phases are chosen during 2014. In order to maintain uniform dataset of near-homogeneous cloud type for each ISM phase category, 11 days from each category are selected. The number of reflectivity profiles associated with the above selected active (246,225) and break (173,784) ISM phases has been utilized for bringing out mean composite diurnal cycle to understand the role of local solar heating and normalized (to substantiate the number of profiles difference) contoured frequency by altitude diagram (CFAD) for statistically reliable characterization of the cloud vertical structure (Houze et al. 2007). Further, the break (active) data statistics for non-precipitating, light-drizzling and heavy-drizzling conditions are found to be around 39 (31)%, 11 (32)% and 2 (14)%, respectively. The non-precipitating clouds are most dominantly seen irrespective of break or active ISM phase but heavy-drizzling precipitating cloud is seldom seen during break ISM phase.

Near-simultaneous along-track observations from space-based CloudSat's CPR over the radar site are used to obtain IWC profiles pertinent to ISM phases. For the comparison in the study, Release 4 2B-CWC-RO data are used. In brief, separate ice and liquid cloud water content retrieval methods in CloudSat use forward model which assumes a lognormal size distribution of cloud particles and active and passive remote sensing data together with a priori data to estimate the parameters of the particle size distribution in each bin containing cloud. CPR measurements provide vertical profile of cloud backscatter; a measured backscatter value and cloud mask (indicate the likelihood that a particular radar bin contains cloud) are obtained from 2B-GEOPROF. Further details, on



Releases 4 of the CloudSat 2B-CWC-RO/RVOD Standard Data Products, can be found in Wood (2008) and Austin et al. (2009). These CPR-retrieved CWC profiles taking into consideration of minimum detectable reflectivity of CPR above -26 dBZ only are used to validate the KaSPR-retrieved microphysical profiles. However, due to the differences in platforms, time resolution, operation strategy, frequency, antenna size and other salient features, exact matching cannot be expected. We only need to confirm the near similarities between simultaneous nadir-looking CPR and zenith-looking KaSPR measurements from the same cloud system. Since CPR has a vertical resolution of 500 m and an along-track resolution is 1.7 km, it takes 15 days to come back to the same location on the globe. That means, in a month two profiles can be gained for a particular location on globe with the narrow swath of CloudSat measurements. Moreover, for comparison, it is necessary to detect the same cloud by both the ground-based KaSPR and space-borne moving CPR. These are the reasons to have very few number of simultaneous cloud microphysical profiles from KaSPR and CPR and hence for the comparison.

During the ISM active (break) period, the maximum cloud zone (ITCZ) of much uniform/homogeneous (isolated) cloud exists over Indian zonal region that ensures to assume that clouds of nearly same type exist along the latitude (Sikka and Gadgil. 1980). Depending on this fact, where CPR data were not available within 30 km ( $\pm 0.3^\circ$ ) vicinity of KaSPR observation, the CPR premises has been extended up to  $1^\circ$  (max  $74.7^\circ\text{E}$ ) along the longitude from the radar location but the latitude is fixed for  $18.03^\circ\text{N}$  ( $\pm .04$ ). Due to the homogeneous cloud-type distribution of monsoon clouds, especially over the Indian west coast region ( $72\text{--}76^\circ\text{E}$  long and  $15\text{--}19^\circ\text{N}$  lat), the same cloud structure can be seen by KaSPR and CPR observations even though they are 100 km apart. Moreover, the chosen IWC profile of CPR is closest best matched profile representing the radar location. This could be the probable reason leading to have good comparison between the KaSPR- and CPR-retrieved IWC profiles. But during some of the break monsoon periods due to the isolated type of cloud cluster presence, the inhomogeneous cloud distribution causes difficulties in comparison between the two observations. Those cases have been not considered for this study.

Along with IWC and LWC, median volume diameter (MVD) can also be retrieved in the same way using empirical relation from earlier studies (Vivekanandan et al. 1999). The droplet size distribution  $N(D)$  can be specified using a modified Gamma distribution

$$N(D) = N_0 D^\alpha \exp(-\Lambda D^\gamma) \tag{6a}$$

where  $\alpha$ ,  $\gamma$ ,  $\Lambda$  and  $N_0$  are the parameters that define the distribution and  $D$  is the droplet diameter. For a given LWC, as the MVD increases, so does the corresponding reflectivity. In the case of a modified Gamma DSD, reflectivity depends on too many parameters of the size distribution and MVD

cannot be retrieved from a reflectivity measurement alone. For the special case of  $\alpha \rightarrow 0$  and  $\gamma \rightarrow 0$ , the DSD becomes an exponential function and can be used to estimate MVD as

$$\text{MVD} = \{2.16 \times 10^{-4} \times (Z/\text{LWC})\}^{1/3} \tag{6b}$$

where MVD is in mm,  $Z$  is in  $\text{mm}^6 \text{m}^{-3}$ , and LWC is in  $\text{gm m}^{-3}$ .

Validation of LWC profiles has been attempted using various observational data. These include aircraft observation collected during Cloud Aerosol Interaction and Precipitation Enhancement Experiment (CAIPEEX) campaign over the radar site and other ground-based complementary observations like microwave radiometer. Aircraft observation helps by directly comparing radar-estimated profiles of LWC and MVD with aircraft-estimated profiles. Since aircraft observation are limited to lower altitude (max 4 km), this indirectly offers validation for LWC profiles only. Like CloudSat, availability of aircraft observations is also very limited.

The ground-based MWR used in this work is a MP-3000A (Radiometrics Corp., USA), 35-channel temperature, water vapor and liquid water profiler. LWP values are estimated using physical iterative method (Han and Westwater 1995; Liljegren et al. 2001). The technique for determining LWC from radar reflectivity and integrated LWP retrieved from microwave radiometer measurements was first presented by Frisch et al. (1995). It was developed further by Frisch et al. (1998) to show that retrieval of the LWC profile does not depend on a lognormal droplet distribution assumption and that the method is independent of radar calibration errors. This retrieval is based on the assumptions that both cloud droplet concentration and the width of the particle size distribution are constant with height. Using these assumptions, it is possible to write the relationship between LWP and  $Z$  as

$$\text{LWC}(h) = \text{LWP} \frac{\sqrt{Z(h_i)}}{\sum_{i=1}^M (\Delta h_i \sqrt{Z_i})} \tag{7}$$

Here,  $i$  is the index of vertical layer, 1 and  $M$  indicate the lowest and the highest vertical range bin, respectively,  $Z$  is in  $\text{mm}^6 \text{m}^{-3}$ , LWP is in  $\text{gm m}^{-2}$  and LWC is in  $\text{gm m}^{-3}$ . LWP profile from MWR is converted into LWC profile using Eq. (7) and is compared to have multi-instrument validation.

### 3 Results and discussion

#### 3.1 Retrieval of IWC profile and its validation with the CPR

Figure 2a shows the vertical profiles of cloud radar reflectivity on June 6, 2015 during 1003–1005 UTC where the

thin cirrus clouds of thickness  $\sim 1$  km centered at  $\sim 13$  km altitude are present. The  $Z$  profiles (six) of every 20 s interval exhibit inconsistency in trend which reflects the high degree of variability of the cloud microphysics. Figure 2b corresponds to IWC profiles estimated using Eqs. (1) and 2, i.e., without (solid lines) and with (dotted lines) temperature correction in estimating IWC. Further, the vertical velocity and spectral width measurements ( $\sim 0.3$  m s $^{-1}$ , not shown here) show the presence of turbulence within cirrus cloud during the observational period. It might be due to the dynamical interaction of cloud with the surroundings through entrainment or turbulence processes which results in the vigorous temporal variability in the  $Z$  profiles. The other case, observed on July 8, 2016 at 0531 UTC, shown in Fig. 2c, d, depicts homogenous cloud which is also confirmed from vertical velocity measurements. So, spectral width values within the observed cirrus are less ( $\sim 0.1$  m s $^{-1}$ ) and its thickness is  $\sim 3$  km centered at an altitude of  $\sim 10$  km. Relatively thicker cirrus cloud of higher reflectivity values (Fig. 2c) will be sustainable against the environmental interactions. Therefore, the  $Z$  and IWC profiles are consistent with each other as seen in Fig. 2d. The temperature-corrected IWC profiles can be seen as dotted profiles in Fig. 2b, d which are more for reflectivity  $< -25$  dBZ, whereas for high reflectivity ( $> -20$  dBZ) they are less than those of IWC retrieved from IWC– $Z$  relationship. According to Protat et al. (2007), due to different formation mechanisms for larger  $Z$  values ( $> -15$  dBZ), different relationship should be used rather than  $Z$ –IWC relationship. To reduce both the systematic overestimation and RMS differences of the small IWCs ( $0.01$  gm m $^{-3}$ ), Protat et al. (2007) emphasized the

use of temperature as an additional constraint in retrieving IWC. However, Fig. 2 shows that the maximum difference between these two retrieved profiles at the center of cirrus cloud in both cases is  $\sim 2$  mg m $^{-3}$ . Thus, henceforth, for simplicity the temperature correction to IWC is not used and is inferred using the  $Z$  value.

IWC profiles retrieved from KaSPR are validated with CPR's IWC profiles confined around the radar site as described in Sect. 2. Further, the cross-comparison between KaSPR- and CPR-measured  $Z$  and IWC profiles is done pertinent to ISM active and break spells to understand the difference between the two phases through the ice microphysical processes. Figure 3a shows the cross-comparison of height profiles of  $Z$  from ground-based KaSPR (solid black line) and space-based CPR (dashed red and gray lines; red line is after applying cloud mask threshold of  $-26$  dBZ, i.e., the minimum detectable reflectivity of CPR) taken on August 17, 2015 around 0840 UTC. Figure 3b is the corresponding IWC profiles comparison between KaSPR and CPR. Both cloud radars (KaSPR and CPR) are able to capture significantly the peak regions of the cirrus cloud with near-similar reflectivity ( $\sim -20$  dBZ). Due to the coarse vertical resolution, the finer fluctuations in IWC profiles are missed out by CPR that can be seen with KaSPR (Fig. 3a). These finer fluctuations in  $Z$  explain the corresponding differences in IWC profiles shown in Fig. 3b. Both time and location considered in this case for both KaSPR and CPR are given in the box. Albeit the differences between the two radars as mentioned earlier, their near-simultaneous cloud measurements are able to show similar gross features of IWC. It confirms the observation of the same cloud by the two radars. Another three cases are studied to bring out the

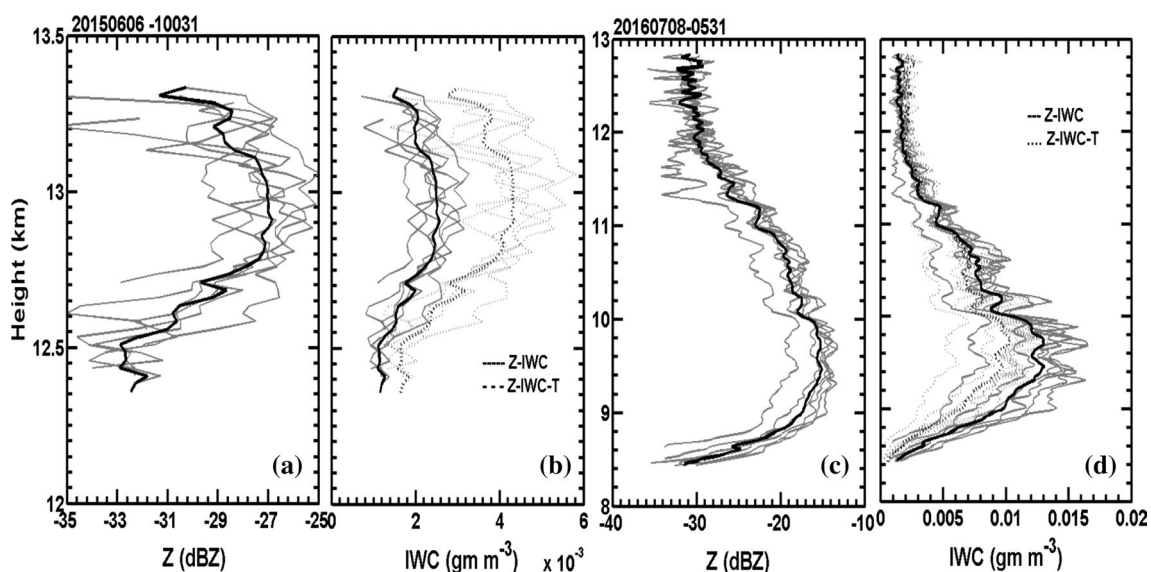
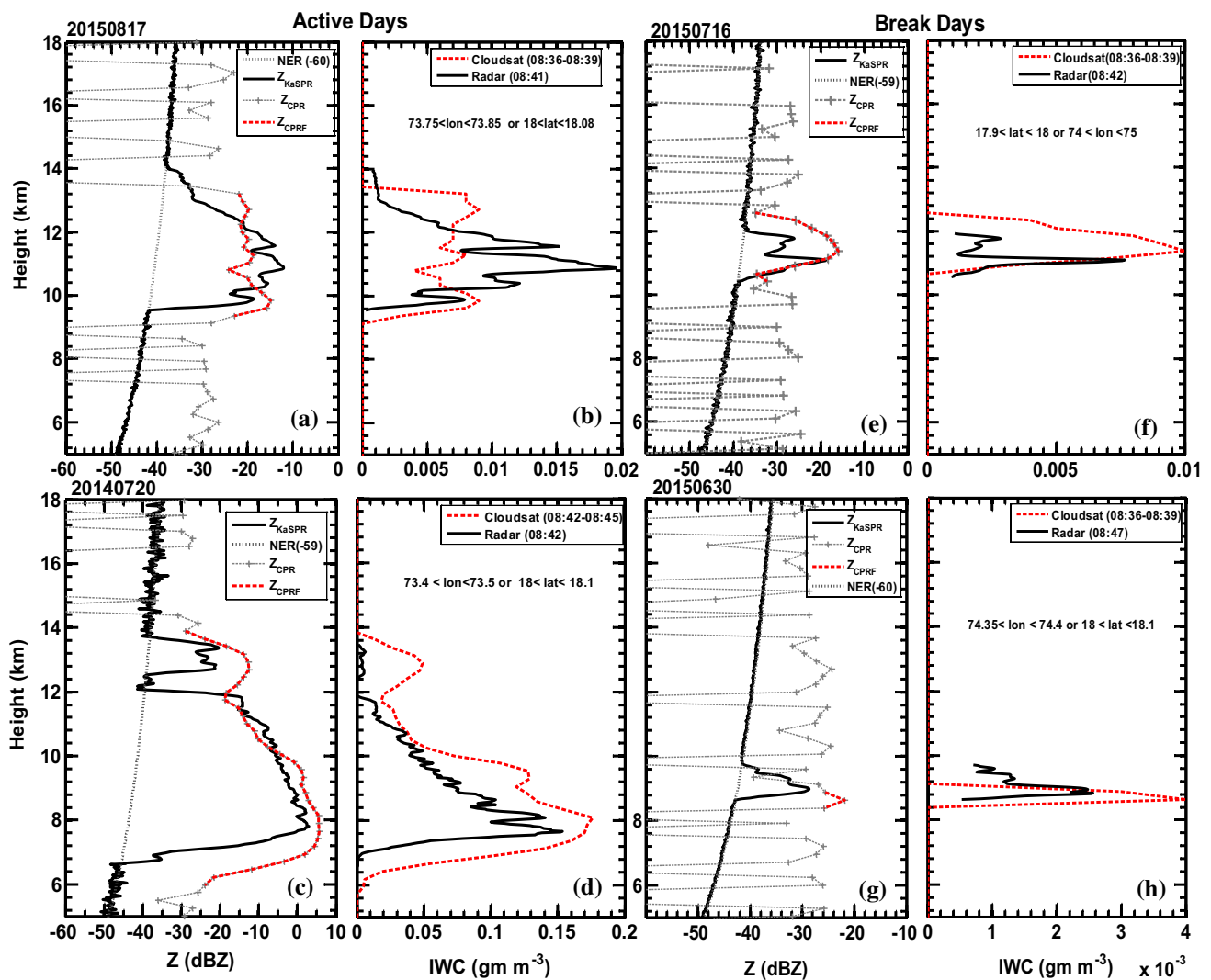


Fig. 2 Vertical profile of a  $Z$  and b IWC retrieved from  $Z$  on June 6, 2015 at 0531 UTC (c, d) same as (a, b) but for July 8, 2016



**Fig. 3** Four comparison cases between space-based cloud profiling radar (CPR) and ground-based KaSPR are on **a, b** August 17, **c, d** July 20, 2014, **e, f** July 16 and **g, h** June 30, 2015. Two left (right)-

side cases representing active (break) ISM period. For each case, left panel shows reflectivity profile comparisons with the noise equivalent reflectivity curves and IWC profile comparison seen in the right panel

general differences pertinent to the active and break phases of ISM besides the comparison of the KaSPR and CPR profiles. Wide (narrow) IWC slab thickness is seen during active (break) phase. This result is consistent with that of Das et al. (2013), which showed that the sub-visible cirrus and thin cirrus are more frequent during the break periods. However, thick and dense cirrus clouds are more frequent during the active periods of monsoon. Mainly, time and location differences involved between KaSPR and CPR observations may cause the difference within the IWC profiles of Fig. 3g. All cases, except August 17, 2015, show overestimation by CPR. One plausible reason could be that the CPR samples over a relatively larger area in short span of time around the radar site. Further, the close agreement (disagreement) of profile trends infers that the observed cloud is possibly a homogeneous (inhomogeneous) cirrus cloud with a prominent peak

confined either at center or bottom of a region favoring the growth of ice.

Figure 4 shows the comprehensive picture of comparison of collocated mean Z and IWC collocated profiles obtained from KaSPR and CPR observed during 2013–2016, in the height region of 5–15 km. The eight Z and corresponding IWC profiles of CPR corroborated with KaSPR measurements over the radar site are used to compute the mean and the standard deviation. The mean Z profiles of KaSPR and CPR are well within the variability of one another. However, the mean IWC profile comparison is good above ~7 km where it shows exponential IWC decay with increasing altitude. The difference of IWC profiles between KaSPR and CPR is mainly due to differences pertinent to the method of IWC estimation between two cloud radars discussed in Sect. 2. However, KaSPR used empirical relation applied to

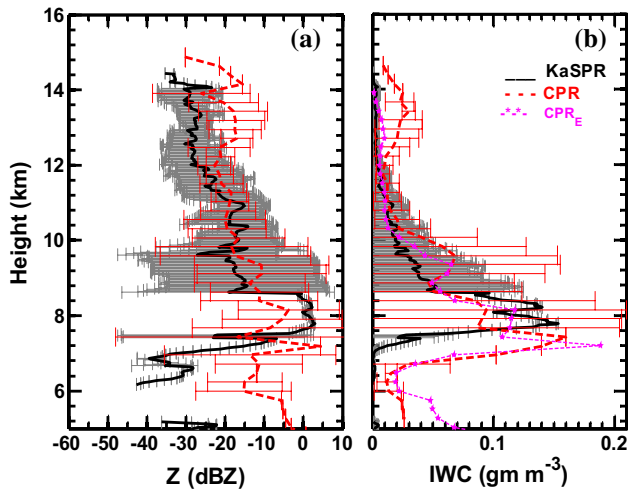


**Fig. 4** **a** Comparison of collocated CPR with the KaSPR mean and standard deviation of reflectivity and **b** IWC profiles for the period 2013–2016

the CPR-measured  $Z$  to have empirical IWC profiles (CPR<sub>E</sub>) that can be seen in Fig. 4b. It is noted that both IWC growth and LWC growth are much vigorous during active days and thus are quantitatively higher than the break days.

### 3.2 Liquid water content profile cross-validation with local aircraft and with other complementary surface observations

To validate the empirically estimated LWC profiles from KaSPR, aircraft observations over radar site during the CAIPEEX have been utilized. Figure 5 shows an event on July 9, 2015, when CAIPEEX aircraft observations were collected over the radar site during 0737–0834 UTC. Figure 5a represents mean vertical profile of reflectivity at 0740 and 0810 UTC each with 150 s duration. The profile at 0740 UTC (red line) has mean reflectivity values below  $-30$  dBZ, which indicates a non-precipitating cloud, whereas the succeeding profile (green dashed line), which has reflectivity value  $\sim -10$  dBZ, implies light drizzling. Equations (3) and (4) are employed for the non-precipitating and light-drizzle case, respectively, to retrieve LWC profiles from KaSPR and are shown in Fig. 5. LWC measured by two different instruments with the aircraft observation, namely hotwire probe and cloud droplet probe (CDP), is depicted in Fig. 5b along with the KaSPR-retrieved LWC profiles. CAIPEEX flight path observations were limited to 4 km, and hence, comparison of the whole LWC profile is not possible here. Figure 5b shows a good agreement between aircraft-based LWC measurements and KaSPR-retrieved LWC for the non-precipitating case. It could be due to the cloud droplet probe's ability to detect smaller sizes. Radar-derived LWC profile for non-precipitating cloud shows good agreement

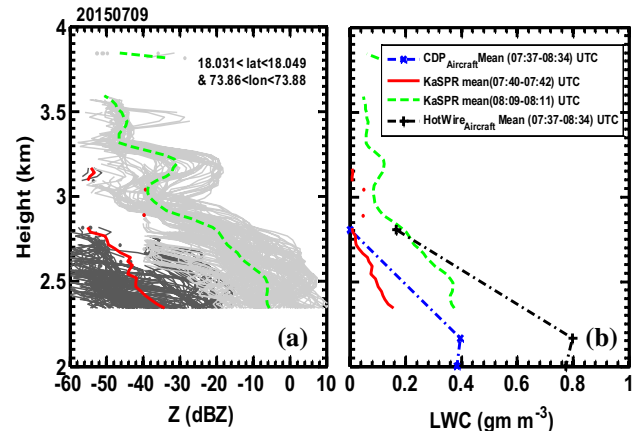


**Fig. 5** Mean vertical profile of **a** radar reflectivity with different colors for different times, vertical mean profile of **b** LWC from CDP and hotwire observations of CAIPEEX aircraft (dash dotted line); the red and green colors lines are for different time means of LWC estimated from radar  $Z$

with LWC profile retrieved from these two instruments. But in case of hotwire (Fig. 5b) which is sensitive to drizzling cloud drops as well, LWC profile during a light-drizzling episode is comparable with the LWC profile retrieved from KaSPR.

Figure 6 shows another example of the radar-derived LWC and aircraft CDP and hotwire probe LWC observations confined around the radar site during 0938–0953 UTC on November 12, 2014. Area covered by the aircraft around the radar is extended from 17.85 to 19.11°N latitudes and 72.74 to 73.96°E longitudes. Figure 6a shows the mean with a spread of instantaneous reflectivity profiles around it. For non-precipitating case, Eq. (3) is used to retrieve LWC. CAIPEEX aircraft observations during 2014 are limited to only CDP and hotwire measurement for LWC profile. However, the main purpose of this comparison is to show that the mean of the radar-estimated LWC profile is well within the range of LWC values from the aircraft measurement. With the help of the KaSPR reflectivity and LWC (non-drizzling condition), MVD has been computed using Eq. (6b). This is compared with the MVD obtained from CDP. Figure 7a shows that the MVD size profiles estimated from KaSPR on July 9, 2015 are comparably in the same range with near-similar trend as that of the CAIPEEX observation. Another comparison of MVD profile has been made during 0938–0953 UT on November 12, 2014 around radar location as shown in Fig. 7b. Radar-estimated MVD values mostly agree with minimum values of MVD observed by aircraft. This infers that clouds over radar location have relatively less LWC than other regions of the flight path.

Complementary local LWP measurements from MWR collocated with KaSPR observations are used in combination with radar reflectivity for estimating LWC by



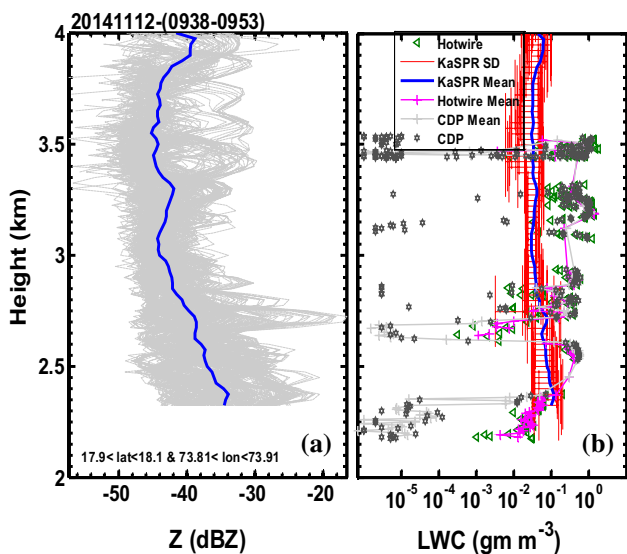
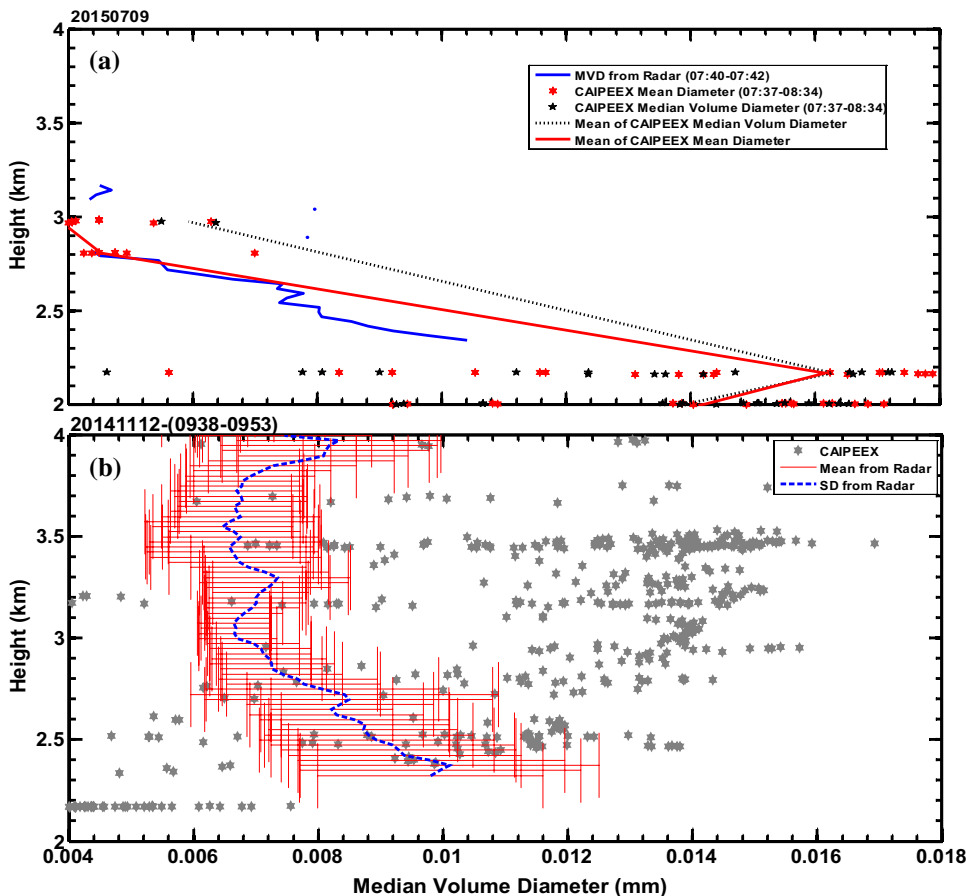


**Fig. 6** Vertical profile of **a** KaSPR reflectivity (bold blue line is mean that passes center to the spread of Z values, **b** LWC profile comparison between CDP, hotwire and KaSPR. KaSPR-estimated LWC mean (blue line) and standard deviation (red error bars) are on November 12, 2014

**Fig. 7** Vertical profile of MVD estimated from radar (blue line), MVD from CAIPEEX (black dotted line) and mean diameter (red line) from CAIPEEX on **a** July 9, 2015 and **b** November 12, 2014



Eq. (7). The LWC profiles retrieved by two methods are cross-compared in Fig. 8. Figure 8a, b shows two non-precipitating episodes, on July 8, 2016 at 0658 and at 1242 UTC. Figure 8c, d shows two light-drizzling episodes, on July 9, 2016 at 0140 and at 1349 UTC. Figure 8e, f shows two heavy-drizzling episodes, on July 9, 2016 at 0841 and July 10, 2016 at 0528 UTC. Even though good agreement is found among the two non-precipitating LWC profiles (e.g., Fig. 8a), the empirically retrieved KaSPR LWC profile yields higher values than the other two. Higher LWC values from KaSPR are justified with its better height and time sampling (i.e., 25 m) MWR (500 m). Finer resolutions actually help to capture more detailed variations of LWC/LWP pertinent to the microphysical process inside the clouds. Systematic degradation of LWC values from KaSPR to MWR seen in Fig. 8a is attributed mainly due to the resolution differences and different evaluation methods. This affects the path-integrated water content measurements. The radar-retrieved LWC is dominant until droplet size enters into Mie scattering region of KaSPR (i.e., 0.8 mm) where cloud radar suffers from attenuation, which can be seen in Fig. 8c, d below 2.8 km and significantly below ~5 km in Fig. 8e, f where at lower

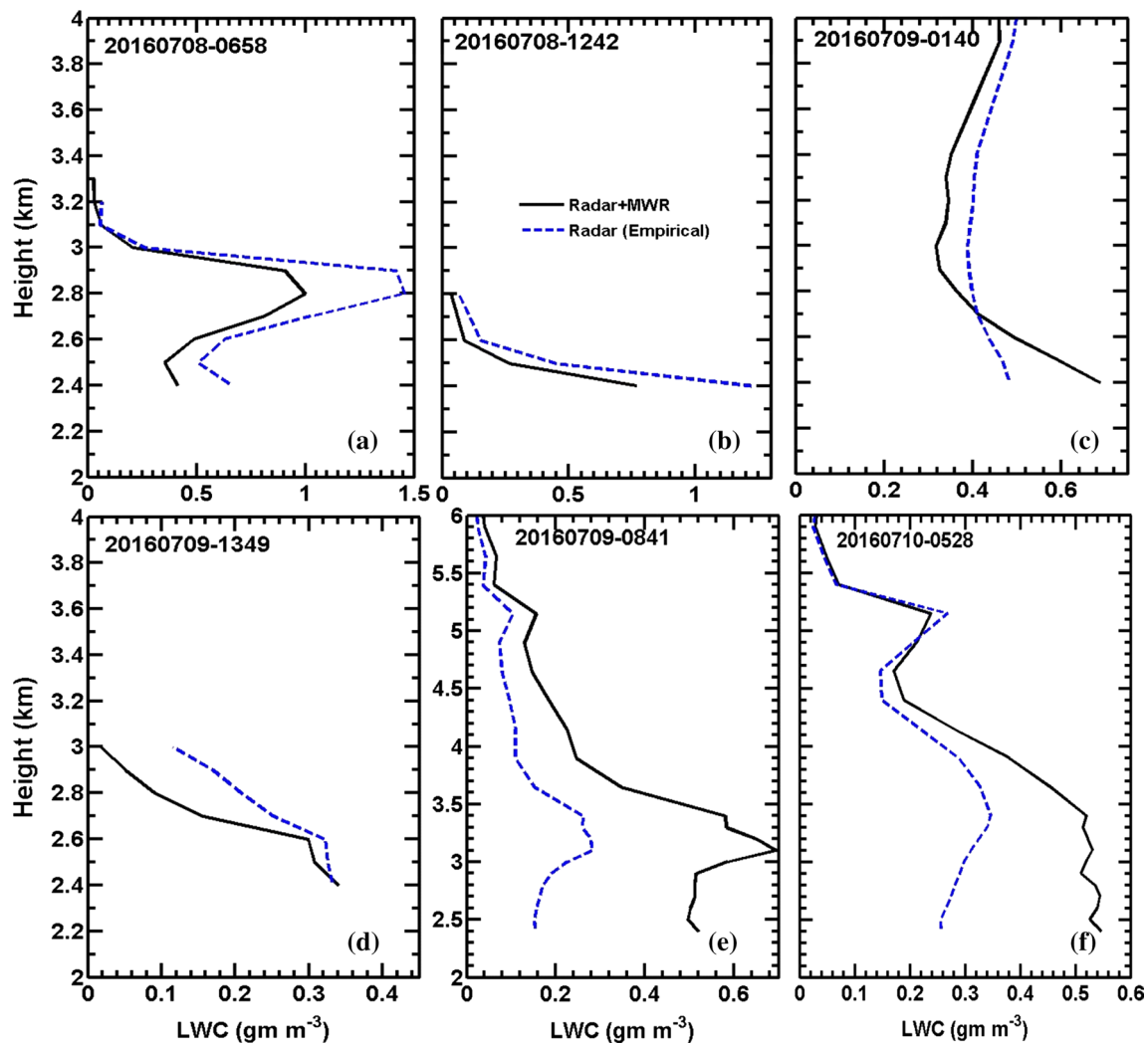


**Fig. 8** Comparison of Z and LWC profiles during **a, b** non-precipitating, **c, d** light-drizzling and **e, f** heavy-drizzling conditions

height region reflectivity values (above 10 dBZ; not shown) are inferring drizzle. This is much more evident in the heavy-drizzling condition where radar attenuation by raindrops is mainly confined below  $\sim 5$  km altitude (Fig. 8e, f). However, in this study we have not attempted rain attenuation correction to KaSPR. It is to be noted that MWR can provide liquid water content but it is incapable of distinguishing the LWC contribution from cloud and rain which is another reason for dominant LWC from MWR during rain condition. Thus, finer resolution radar-retrieved cloud LWC is more accurate and less biased. The exception is during precipitation where rain attenuation correction needs to be applied. If this is not done, raindrop-affected reflectivity measurements show apparent lower LWC values. The difference mentioned above might also be originated from the imperfect Z–LWC relationships, other than resolution and attenuation.

### 3.3 Composite diurnal evolution for topical vertical structures of cloud IWC pertinent to active and break ISM spells

Hourly average KaSPR data analysis has been done to bring out the composite diurnal cycle to see the cloud evolution with respect to the local solar heating response. In fact, according to Stull (1990), hourly timescale is the response of atmospheric boundary layer, the lowest layer of turbulent atmosphere which is directly influenced by the solar radiation. Thus, the composite diurnal analyses associated with IWC and LWC are prepared by considering hourly averaged KaSPR vertical profiles for the present study. Even half-hourly averages have also been computed, and it has been found that the gross features are not much significantly different from hourly average data. Further, the composite has been taken for the active and break days followed by IMD. In Fig. 9a, the composite diurnal of IWC

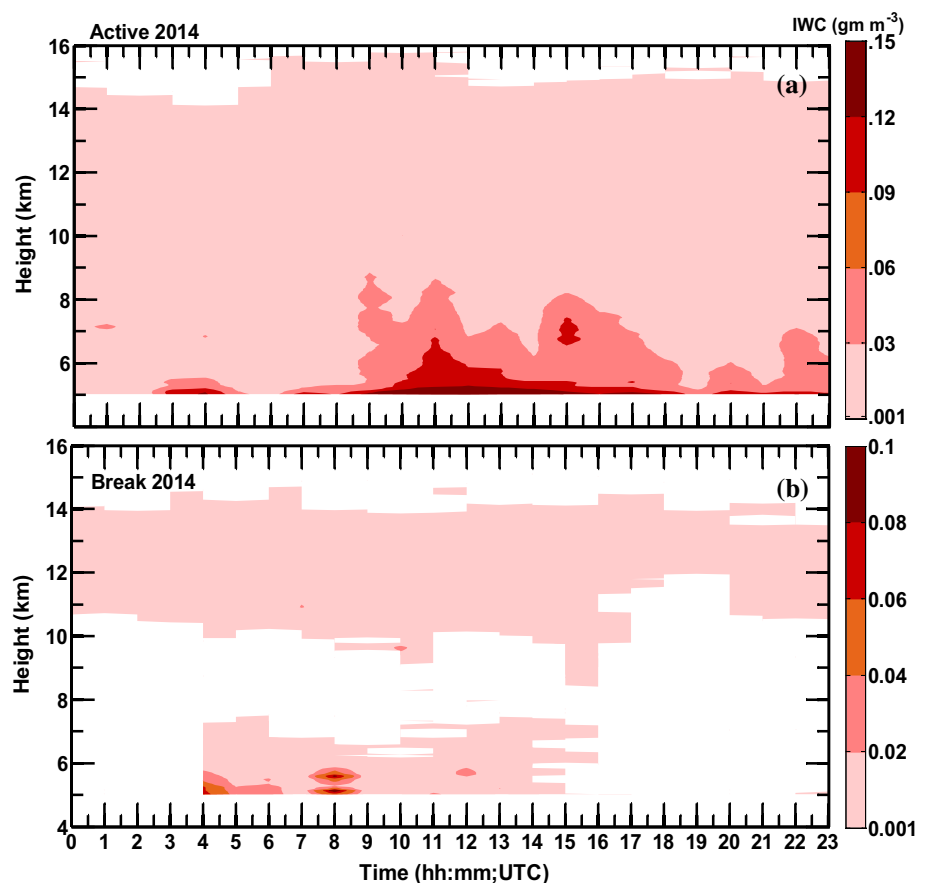
profile during active ISM period shows higher IWC values exist below 8 km and weak IWC concentrations are seen at higher level cirrus (above 10 km). It ultimately results in five times higher ( $\sim 0.15 \text{ gm m}^{-3}$ ) IWC than the upper level IWC ( $0.05 \text{ gm m}^{-3}$ ) which settles down around the time (10–14 UTC, the local time in this region = UTC + 5 h.) when surface heating gets maxima due to solar insolation. On the other hand, discontinuous cloud vertical structure during break monsoon days shows existence of two layers where the upper layer (> 10 km) cirrus presence is similar to that of the active phase. But unlike active days, break days lack the interaction between the two levels which limits the IWC value below  $0.02 \text{ gm m}^{-3}$  and also its duration by the presence of solar radiation. Das et al. (2013) showed near-similar IWC features during active and break ISM phases over the Central India using CPR but their IWC values were at least four times smaller. The strong diurnal variation seen with higher IWC values indicates the role of lower level convective activity that is more vigorous during active period than the break period. Vertical velocity observations below 10 km show downdraft velocities more than  $1.5 \text{ m s}^{-1}$  are always present throughout the day, which increase up to  $-4.5 \text{ m s}^{-1}$  below 6 km during active time as shown in Fig. A1(b). In contrast, during break period, downward vertical velocities never exceed  $-1.5 \text{ m s}^{-1}$ , signifying the presence of the

small particles in this time (Fig. A2(b)). The small particle size is confirmed from reflectivity value in Fig. A1(a) which is below  $-24 \text{ dBZ}$  most of the time. On the other hand, the distribution of domination of big-sized particles during active days is evident from the reflectivity values which are ascending gradually at the lower level.

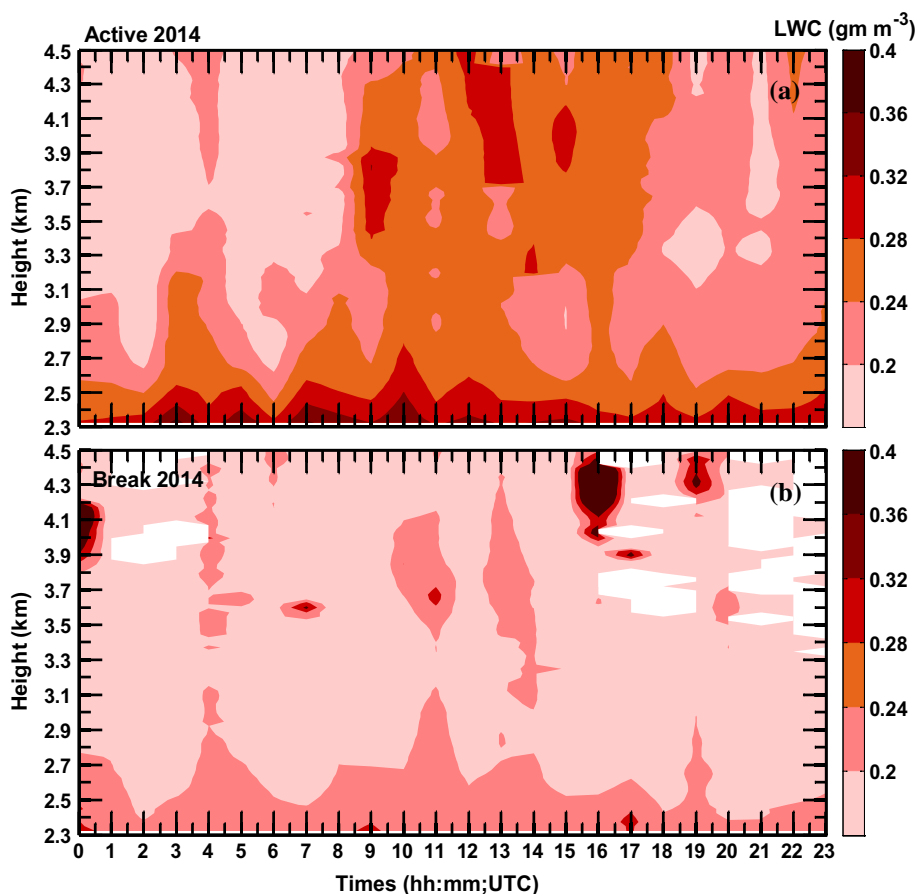
### 3.4 Composite diurnal evolution of vertical structures of cloud LWC pertinent to ISM active and break spells

Figure 10 shows the hourly mean composite diurnal of LWC profile associated with the active and break ISM phases. This diurnal is composed on the basis of mean Z measurements of the lowest three range bins that follow the defined class of cloud (non-precipitating, light drizzling and heavy drizzling) discussed in Sect. 2. The independent diurnal prepared for non-precipitating, light- and heavy-drizzling condition has been further composited to bring out a single-composite diurnal for LWC. The higher LWC values are mostly confined below 2.8 km during both the ISM phases. LWC values greater than  $0.24 \text{ gm m}^{-3}$  are mostly missing during break ISM, whereas those values are predominant in the warm cloud region during active ISM days. At local 14–22 h, a convective activity can be seen during active days

Fig. 9 HTI plot of composite diurnal of IWC for a active and b break ISM periods of 2014



**Fig. 10** Composite diurnal of LWC for **a** active and **b** break ISM periods of 2014



where LWC value more than  $0.28 \text{ gm m}^{-3}$  is observed at the height of 4 km or more which is missing in the break days. This strong LWC column response is mostly attributed to the local solar heating. Unlike break days, amount of LWC during active days can reach up to  $0.4 \text{ gm m}^{-3}$  or more especially before local late evening hours (15 UTC). The secondary peaks in LWC values at higher heights are mostly contributed by non-precipitating clouds in both active and break periods. It infers that this typical local diurnal feature might be arising due to the fall of temperatures during late evening hours that favors the slightly improved LWC values by the water vapor saturation with non-precipitating clouds. Further, radar-measured downward velocity ( $> 4 \text{ ms}^{-1}$ ) associated with active days (not shown) infers the fall of relatively big-sized particle toward surface which is unlikely during break days. Further, KaSPR measurement on cloud tops, during the break ISM period, rarely exceeds 4 km altitude and most of the time it is below  $\sim 3 \text{ km}$  AMSL which infers that the break ISM period clouds generation is due to weak convection. Another important feature which has been noted is the high spectral width (with non-precipitating clouds) values during active phase ( $> 1 \text{ m s}^{-1}$ ) indicating the dominance of higher turbulence activity associated with

warm- or low-level cloud that favors the collision and coalescence processes.

From the above composite diurnal analysis on IWC and LWC, an attempt is made here on linking the complete cloud water content (IWC + LWC) profile that allows to access the complete cloud vertical structure. It helps to understand the role of ice and liquid microphysical growth process which is involved in the initiation of consequent ISM precipitation process. The maximum IWC growth is seen during the diurnal maximum solar insolation period around 9–13 UTC, and closely around similar period, there exist maxima in LWC during the light drizzling and heavy drizzling. Light drizzling picks up around 8 UTC, and later it transforms into heavy drizzling after 9 UTC. Further, such favorable microphysical profile diurnal feature is not expected during ISM break phase due to two reasons (1) weak or complete absence of clouds in between 8 and 10 km and (2) missing of sharp increase in ice microphysical process (IWC growth) feature below 8 km. Peak IWC values during ISM active phase exhibit five times higher values than the ISM break. Moreover, the rain accumulation at radar site during all chosen active (161.6 mm) days is more than three times higher than the break (46.7 mm) days in 2014. The lidar observations of cirrus clouds presented by Grund et al. (2001)



also discussed the fallout/escape of bigger ice crystals from cirrus base that can act as seeding agent for the underlying warm clouds to invigorate. Thus, it can be concluded that ice microphysics plays an important role for the warm cloud invigoration and initiation of ISM precipitation lying beneath the lower level cloud.

### 3.5 Evaluation of IWC and LWC obtained from reanalysis data with respect to KaSPR

In order to evaluate the model-retrieved microphysical properties, European Centre for Medium-Range Weather Forecasts (ECMWF) reanalysis data (ERA-Interim; Dee et al. 2011) at  $0.125^\circ \times 0.125^\circ$  resolution has been utilized to obtain IWC and LWC profiles for same active and break ISM days considered in this study, as shown in Fig. 11a–d, respectively. Figure 11 indicates there is an overestimation

of IWC during active days, whereas for break days, reanalysis data underestimate the value compared to the KaSPR but are able to show cloud vertical structure discontinuity during break period. For LWC, model-retrieved values are much smaller than KaSPR (Fig. 11c, d), and it is unable to show any contrast between active and break days below 2 km where KaSPR measurements are absent. This could be due to the huge area coverage of model-retrieved profiles, trading off the ability to capture small-scale details. The reanalysis data are also derived in an interval of 6 h, thus lacking the high-resolution timescale facility necessary to study cloud microphysical properties. KaSPR and ERA-Interim show different diurnal variations.

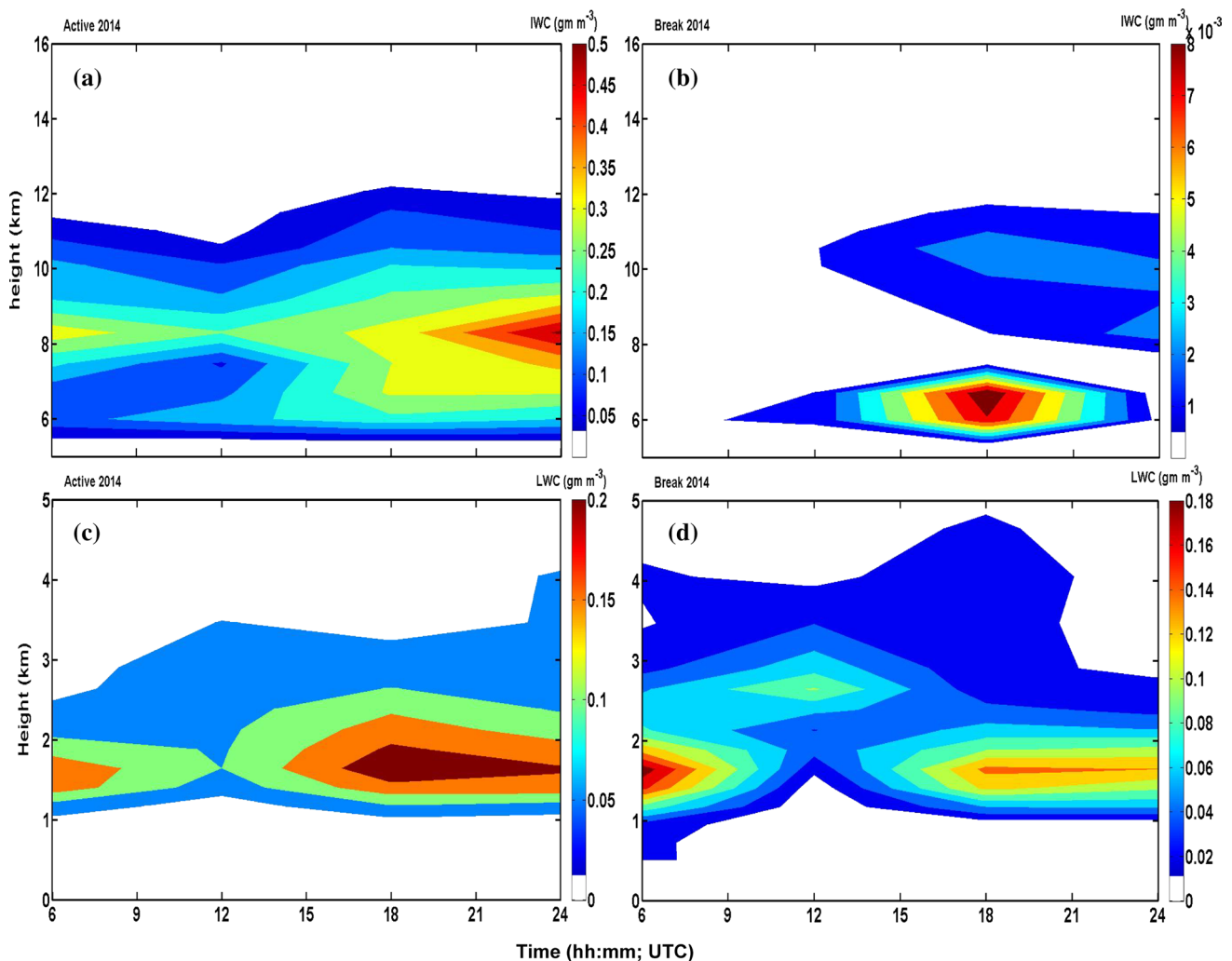


Fig. 11 Contour plot of composite diurnal of a, b IWC c, d LWC for ISM active and break days, respectively, using ECMWF reanalysis

### 3.6 CFAD analysis of cloud IWC and LWC profiles pertinent to ISM active and break spells

Contoured frequency by altitude diagram (CFAD) involves histogram analysis of required parameter for every height level in the vertical profile. Normalized CFAD analyses adopted here permit the comparison of CFADs between different altitude regions/layers within the composed cloud vertical structure despite the different absolute frequencies (Houze et al. 2007). In fact, this allows further connection between the active and break ISM CFADs as well. CFAD for cloud LWC and IWC for 11 active and break ISM days have been obtained. There exist more than 1000 profiles per hour measurement of KaSPR. Figure 12 shows the CFAD analysis during active and break ISM phases, for IWC as well for LWC. For active days, maximum occurrence of IWC is confined around 10–16 km or above (Fig. 12a) but in break days it is limited within 12–13 km (Fig. 12b). One order difference in magnitude of IWC values between active and break ISM phases is evident. Significant contrast is found out in the maximum occurrence of LWC value in these two ISM phases (Fig. 12c, d). Due to the presence of convective activity in the active days, up to 50% of cloud occurrence can be found above 4 km (Fig. 12c) which is blocked at 3.2 km for break days (Fig. 12d). The highest cloud water

content values show widespread distribution with either falling/sloping down (near uniform; see Fig. 12a, c), with increasing height (see Fig. 12c) or confined flat as cirrus layer (see Fig. 12b). Peculiar behavior of LWC during active ISM (below  $0.4 \text{ gm m}^{-3}$ ) may be due to the involvement of the non-precipitating with precipitating cloud that needs to be understood further.

## 4 Summary and conclusions

A first attempt is made to understand the microphysical vertical structure and evolution in clouds during different phases of monsoon over the monsoon region of India using ground-based cloud radar. Earlier studies on monsoon cloud microphysical structures are carried out using space-based radar which is able to detect only the gross large-scale microphysical properties during ISM phases. High-resolution, vertical-looking radar observation helps to capture the microscale changes associated with monsoon cloud systems. IWC and LWC are estimated mainly using KaSPR reflectivity. Empirical relations between radar reflectivity and cloud IWC/LWC (single relationship for Z–IWC and three different relationships for Z–LWC, depending on the condition of rain) are used. Radar-derived IWC profiles are validated against CloudSat CPR data, whereas LWC profiles are validated using the collocated complementary measurements of microwave radiometer and in situ aircraft observations. Active and break ISM days have been adopted from Indian Meteorological Department (IMD) report. During break period, cloud top heights in the warm regions are limited below 2–3 km (maximum 6 km) signifying the fact that their generation is limited to local convection. Break period lacks the sufficient water content required for the growth and sustenance of deep clouds. The effect of diurnal heating on convection and consequent precipitation results in an afternoon and late-night maxima in the composite diurnal evolution of radar-retrieved liquid water content. This study also shows that variations in IWC, thickness, etc., of ice clouds act as key factors to depict the contrast between the two phases of monsoon. Despite being a point observation, the uniqueness of this study is that it captures the associated large-scale monsoon features over the site in terms of radar-measured variables.

**Acknowledgements** IITM is an autonomous organization that is fully funded by MOES, Govt. of India. Authors are thankful to director, IITM, not only for his wholehearted support for strengthening the radar program but also for monitoring and mentoring the radar research to the next heights. The authors are highly indebted to G. Pandithurai for the discussions and encouragement provided on the research work. We are equally grateful to all those who were involved and helped in setting up and running the IITM's Cloud Radar Facility. KaSPR design and development was done at M/s ProSensing. Authors are grateful to CAIPEEX team for the aircraft observations. The CloudSat

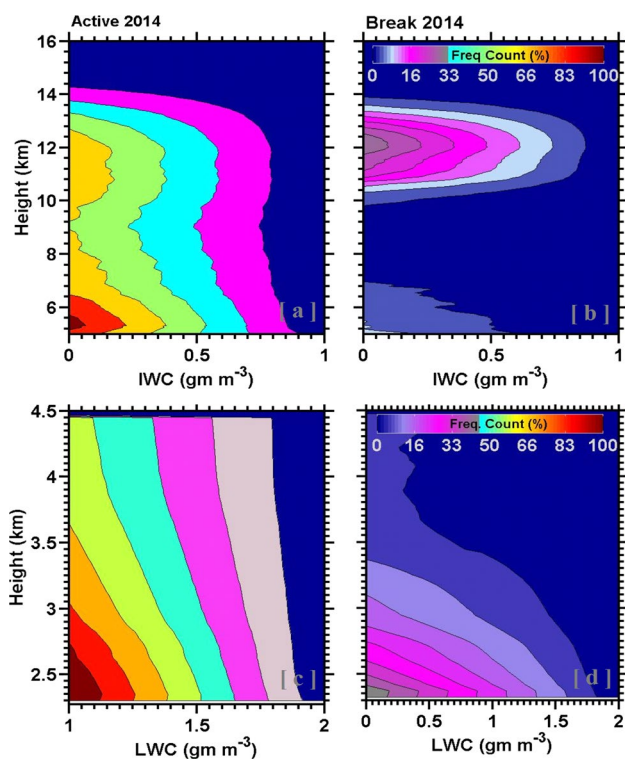


**Fig. 12** Normalized contour frequency by altitude diagram: (a, b) IWC, (c, d) LWC for ISM active and break days, respectively, during 2014

data were obtained from their Web page at <http://www.cloudsat.cira.colostate.edu/data-products>) and ERA-Interim data from the ECMWF (<http://apps.ecmwf.int/datasets/>). The data supporting this article can be requested to the IITM radar data portal or corresponding author (kalapureddy1@gmail.com). We are grateful to MAAP reviewers for their constructive comments and concern for quality that helped to hone the presentation outlook of this work and editor and their team for their all value services.

## References

- Abhik S, Halder M, Mukhopadhyay P, Jiang X, Goswami BN (2013) A possible new mechanism for northward propagation of boreal summer intraseasonal oscillations based on TRMM and MERRA reanalysis. *Clim Dyn*. <https://doi.org/10.1007/s00382-012-1425-x>
- Atlas D (1954) The estimation of cloud parameters by radar. *J Meteorol*. <https://doi.org/10.1175/1520-0469>
- Austin RT, Heymsfield AJ, Stephens GL (2009) Retrieval of ice cloud microphysical parameters using the CloudSat millimeter-wave radar and temperature. *J Geophys Res Atmos*. <https://doi.org/10.1029/2008JD010049>
- Baedi RJP, de Wit JJM, Russchenberg HWJ, Erkelens JS, Baptista JP (2000) Estimating effective radius and liquid water content from radar and lidar based on the CLARE98 data-set. *Phys Chem Earth B*. [https://doi.org/10.1016/S1464-1909\(00\)00152-0](https://doi.org/10.1016/S1464-1909(00)00152-0)
- Baedi R, Boers R, Russchenberg H (2002) Detection of boundary layer water clouds by space borne cloud radar. *J Atmos Ocean Technol*. <https://doi.org/10.1175/1520-0426>
- Das SK, Uma KN, Konwar M, Raj PE, Deshpande SM, Kalapureddy MCR (2013) CloudSat–CALIPSO characterizations of cloud during the active and the break periods of Indian summer monsoon. *J Atmos Solar Terr Phys*. <https://doi.org/10.1016/j.jastp.2013.02.016>
- Dee DP, Uppala SM, Simmons AJ, Berrisford P, Poli P, Kobayashi S, Andrae U, Balsameda MA, Balsamo G, Bauer DP, Bechtold P (2011) The ERA-Interim reanalysis: configuration and performance of the data assimilation system. *Q J R Meteorol Soc*. <https://doi.org/10.1002/qj.828>
- Devasthale A, Grassl H (2009) A daytime climatological distribution of high opaque ice cloud classes over the Indian summer monsoon region observed from 25-year AVHRR data. *Atmos Chem Phys*. <https://doi.org/10.5194/acp-9-4185-2009>
- Donovan DP, Lammeren ACAP (2001) Cloud effective particle size and water content profile retrievals using combined lidar and radar observations: 1. Theory and examples. *J Geophys Res Atmos*. <https://doi.org/10.1029/2001JD900243>
- Donovan DP, Lammeren ACAP, Hogan RJ, Russchenberg HWJ, Apituley A, Francis P, Testud J, Pelon J, Quante M, Goddard J (2001) Cloud effective particle size and water content profile retrievals using combined lidar and radar observations: 2. Comparison with IR radiometer and in situ measurements of ice clouds. *J Geophys Res Atmos*. <https://doi.org/10.1029/2001JD900241>
- Ellis SM, Vivekanandan J (2011) Liquid water content estimates using simultaneous S and  $K_a$  band radar measurements. *Radio Sci*. <https://doi.org/10.1029/2010RS004361>
- Fox NI, Illingworth AJ (1997) The retrieval of stratocumulus cloud properties by ground-based cloud radar. *J Appl Meteorol*. [https://doi.org/10.1175/1520-0450\(1997\)036%3c0485:TROSCP%3e2.0.CO;2](https://doi.org/10.1175/1520-0450(1997)036%3c0485:TROSCP%3e2.0.CO;2)
- Frisch AS, Fairall CW, Snider JB (1995) Measurements of stratus cloud and drizzle parameters in ASTEX with a Ka-band Doppler radar and microwave radiometer. *J Atmos Sci*. [https://doi.org/10.1175/1520-0469\(1995\)052%3c2788:MOSCAD%3e2.0.CO;2](https://doi.org/10.1175/1520-0469(1995)052%3c2788:MOSCAD%3e2.0.CO;2)
- Frisch AS, Feingold G, Fairall CW, Uttal T, Snider JB (1998) On cloud radar and microwave radiometer measurements of stratus cloud liquid-water profiles. *J Geophys Res*. <https://doi.org/10.1029/98JD01827>
- Frisch AS, Martner BE, Djalalova I, Poellot MR (2000) Comparison of radar/radiometer retrievals of stratus cloud liquid-water content profiles with in situ measurements by aircraft. *J Geophys Res*. <https://doi.org/10.1029/2000JD900128>
- Gadgil S (2003) The Indian monsoon and its variability. *Annu Rev Earth Planet Sci*. <https://doi.org/10.1146/annurev.earth.31.100901.141251>
- Gaussiat N, Sauvageot H, Illingworth AJ (2003) Cloud liquid water and ice content retrieval by multi-wavelength radar. *J Atmos Ocean Technol* 20:1264–1275. [https://doi.org/10.1175/1520-0426\(2003\)020%3c1264:CLWAIC%3e2.0.CO;2](https://doi.org/10.1175/1520-0426(2003)020%3c1264:CLWAIC%3e2.0.CO;2)
- Gossard EE, Snider JB, Clothiaux EE, Martner B, Gibson JS, Kropi RA, Frisch AS (1997) The potential of 8-mm radars for remotely sensing cloud drop size distributions. *J Atmos Ocean Technol*. [https://doi.org/10.1175/1520-0426\(1997\)014%3c0076:TPOMRF%3e2.0.CO;2](https://doi.org/10.1175/1520-0426(1997)014%3c0076:TPOMRF%3e2.0.CO;2)
- Goswami BN, Ajaya Mohan RS (2001) Intraseasonal oscillations and interannual variability of the Indian summer monsoon. *J Clim*. [https://doi.org/10.1175/1520-0442\(2001\)014%3c1180:IOAIVO%3e2.0.CO;2](https://doi.org/10.1175/1520-0442(2001)014%3c1180:IOAIVO%3e2.0.CO;2)
- Goswami BN, Ajayamohan RS, Xavier PK, Sengupta D (2003) Clustering of synoptic activity by Indian summer monsoon intraseasonal oscillations. *Geophys Res Lett*. <https://doi.org/10.1029/2002GL016734>
- Grund CJ, Banta RM, George JL, Howell JN, Post MJ, Richter RA, Weickmann AM (2001) High-resolution Doppler lidar for boundary layer and cloud research. *J Atmos Ocean Technol* 18(3):376–393
- Han Y, Westwater ER (1995) Remote sensing of tropospheric water vapor and cloud liquid water by integrated ground-based sensors. *J Atmos Ocean Technol* 12(5):1050–1059
- Hazra A, Chaudhari HS, Saha SK, Pokhrel S (2017) Effect of cloud microphysics on Indian summer monsoon precipitating clouds: a coupled climate modeling study. *J Geophys Res Atmos*. <https://doi.org/10.1002/2016JD026106>
- Heymsfield A, Miloshevich JLM, Schmitt C, Bansemmer A, Twohy C, Poellot MR, Fridlind A, Gerber H (2005) Homogeneous ice nucleation in subtropical and tropical convection and its influence on cirrus anvil microphysics. *J Atmos Sci*. <https://doi.org/10.1175/JAS-3360.1>
- Hogan RJ, Gaussiat N, Illingworth AJ (2005) Stratocumulus liquid water content from dual-wavelength radar. *J Atmos Ocean Technol*. <https://doi.org/10.1175/JTECH1768.1>
- Hogan RJ, Mittermaier MP, Illingworth AJ (2006) The retrieval of ice water content from radar reflectivity factor and temperature and its use in evaluating a mesoscale model. *J Appl Meteorol Clim*. <https://doi.org/10.1175/JAM2340.1>
- Houze RA, Wilton DC, Smull BF (2007) Monsoon convection in the Himalayan region as seen by the TRMM precipitation radar. *Q J R Meteorol Soc* 133(627):1389–1411
- Intrieri JM, Stephens GL, Eberhard WL, Uttal T (1993) A method for determining cirrus cloud particle sizes using lidar and radar backscatter technique. *J Appl Meteorol*. [https://doi.org/10.1175/1520-0450\(1993\)032%3c1074:AMFDCC%3e2.0.CO;2](https://doi.org/10.1175/1520-0450(1993)032%3c1074:AMFDCC%3e2.0.CO;2)
- Kalapureddy MCR, Rao DN, Jain AR, Ohno Y (2007) Wind profiler observations of a monsoon low-level jet over a tropical Indian station. *Ann Geophys*. <https://doi.org/10.5194/angeo-25-2125-2007>
- Kalapureddy MCR, Sukanya P, Das SK, Deshpande SM, Pandithurai G, Pazamany AL, Ambuj KJ, Chakravarty K, Kalekar P, Devisetty HK, Annam S (2018) A simple biota removal algorithm for 35 GHz cloud radar measurements. *Atmos Meas Tech*. <https://doi.org/10.5194/amt-11-1417-2018>



- Khain A, Pinsky M, Magaritz L, Krasnov O, Russchenberg HWJ (2008) Combined observational and model investigations of the Z–LWC relationship in stratocumulus clouds. *J Appl Meteorol Climatol*. <https://doi.org/10.1175/2007JAMC1701.1>
- Kollias P, Clothiaux E, Miller M, Albrecht B, Ackerman GT (2007) Millimeter-wavelength radars: new frontier in atmospheric cloud and precipitation research. *Bull Am Meteorol Soc* 88:1608–1624
- Konwar M, Das SK, Deshpande SM, Chakravarty K, Goswami BN (2014) Microphysics of clouds and rain over the Western Ghat. *J Geophys Res Atmos*. <https://doi.org/10.1002/2014JD021606>
- Krasnov OA, Russchenberg HWJ (2002) The relation between the radar to lidar ratio and the effective radius of droplets in water clouds: an analysis of statistical models and observed drop size distributions. In: 11th conference on cloud physics. American Meteorological Society, Ogden UT, p 1.7 (**preprint**)
- Liljegren JC, Clothiaux EE, Mace GG, Kato S, Dong X (2001) A new retrieval for cloud liquid water path using a ground-based microwave radiometer and measurements of cloud temperature. *J Geophys Res Atmos* 106(D13):14485–14500
- Liou KN (1992) Radiation and cloud processes in the atmosphere theory, observation, and modeling. Oxford University Press, New York
- Liu CL, Illingworth AJ (2000) Toward more accurate retrievals of ice water content from radar measurements of clouds. *J Appl Meteorol*. [https://doi.org/10.1175/1520-0450\(2000\)039%3c1130:TMAROI%3e2.0.CO;2](https://doi.org/10.1175/1520-0450(2000)039%3c1130:TMAROI%3e2.0.CO;2)
- Mace GG, Sassen K (2000) A constrained algorithm for retrieval of stratocumulus cloud properties using solar radiation microwave radiometer and millimeter cloud radar data. *J Geophys Res* 105:29099–29108. <https://doi.org/10.1029/2000JD900403>
- Mace GG, Ackerman TP, Minnis P, Young DF (1998) Cirrus layer microphysical properties derived from surface-based millimeter radar and infrared interferometer data. *J Geophys Res*. <https://doi.org/10.1029/98JD02117>
- Matrosov SY (1997) Variability of microphysical parameters in high-altitude ice clouds: results of the remote sensing method. *J Appl Meteorol*. <https://doi.org/10.1175/1520-0450-36.6.633>
- Matrosov SY (1999) Retrievals of vertical profiles of ice cloud microphysics from radar and IR measurements using tuned regressions between reflectivity and cloud parameters. *J Geophys Res Atmos*. <https://doi.org/10.1029/1999JD900244>
- Nair AKM, Rajeev K, Mishra MK, Thampi BV, Parameswaran K (2012) Multiyear lidar observations of the descending nature of tropical cirrus clouds. *J Geophys Res Atmos*. <https://doi.org/10.1029/2011JD017406>
- Pai DS, Sridhar L, Kumar R (2016) Active and break events of Indian summer monsoon during 1901–2014. *Clim Dyn*. <https://doi.org/10.1007/s00382-015-2813-9>
- Protat A, Delanoe J, Bouniol D, Heymsfield AJ, Bansemer A, Brown P (2007) Evaluation of ice water content retrievals from cloud radar reflectivity and temperature using a large airborne in situ microphysical database. *J Appl Meteorol Clim*. <https://doi.org/10.1175/JAM2488.1>
- Raghavan K (1973) Break-monsoon over India. *Mon Weather Rev* 101(1):33–43
- Rajeevan M, Gadgil S, Bhate J (2010) Active and break spells of the Indian summer monsoon. *J Earth Syst Sci*. <https://doi.org/10.1007/s12040-010-0019-4>
- Rajeevan M, Rohini P, Kumar KN, Srinivasan J, Unnikrishnan CK (2013) A study of vertical cloud structure of the Indian summer monsoon using CloudSat data. *Clim Dyn*. <https://doi.org/10.1007/s00382-012-1374-4>
- Ravikiran V, Rajeevan M, Rao SVB, Rao NP (2009) Analysis of variations of cloud and aerosol properties associated with active and break spells of Indian summer monsoon using MODIS data. *Geophys Res Lett* 36:L09706. <https://doi.org/10.1029/2008GL037135>
- Sassen K (2002) In: Lynch DK et al (eds) Cirrus clouds: a modern perspective in Cirrus. Oxford University Press, New York, pp 11–40
- Sassen K, Liao L (1996) Estimation of cloud content by W-band radar. *J Appl Meteorol*. [https://doi.org/10.1175/1520-0450\(1996\)035%3c0932:EOCCBW%3e2.0.CO;2](https://doi.org/10.1175/1520-0450(1996)035%3c0932:EOCCBW%3e2.0.CO;2)
- Sassen K, Mace GG, Wang Z, Poellot MR, Sekelsky SM, McIntosh RE (1999) Continental stratus clouds: a case study using coordinated remote sensing and aircraft measurements. *J Atmos Sci*. [https://doi.org/10.1175/1520-0469\(1999\)056%3c2345:CSCAS%3e2.0.CO;2](https://doi.org/10.1175/1520-0469(1999)056%3c2345:CSCAS%3e2.0.CO;2)
- Sauvageot H, Omar J (1987) Radar reflectivity of cumulus clouds. *J Atmos Ocean Technol*. [https://doi.org/10.1175/1520-0426\(1987\)004%3c0264:RROCC%3e2.0.CO;2](https://doi.org/10.1175/1520-0426(1987)004%3c0264:RROCC%3e2.0.CO;2)
- Sayres DS, Smith JB, Pittman JV, Weinstock EM, Anderson JG, Heymsfield G, Fridlind L, LiAM, Ackerman AS (2008) Validation and determination of ice water content-radar reflectivity relationships during CRYSTAL-FACE: flight requirements for future comparisons. *J Geophys Res*. <https://doi.org/10.1029/2007JD008847>
- Sekelsky SM, Ecklund WL, Firda JM, Gage KS, McIntosh RE (1999) Particle size estimation in ice-phase clouds using multifrequency radar reflectivity measurements at 95.33 and 2.8 GHz. *J Appl Meteorol*. [https://doi.org/10.1175/1520-0450\(1999\)038%3c0005:PSEIIP%3e2.0.CO;2](https://doi.org/10.1175/1520-0450(1999)038%3c0005:PSEIIP%3e2.0.CO;2)
- Sengupta K, Dey S, Sarkar M (2013) Structural evolution of monsoon clouds in the Indian CTCZ. *Geophys. Res Lett*. <https://doi.org/10.1002/grl.50970>
- Sikka DR, Gadgil S (1980) On the maximum cloud zone and the ITCZ over Indian longitudes during the southwest monsoon. *Mon Weather Rev*. [https://doi.org/10.1175/1520-0493\(1980\)108%3c1840:OTMCZA%3e2.0.CO;2](https://doi.org/10.1175/1520-0493(1980)108%3c1840:OTMCZA%3e2.0.CO;2)
- Stull RB (1990) An introduction to boundary layer meteorology. Kluwer, Boston, pp 500–522
- Sui CH, Li X, Yang MJ, Huang HL (2005) Estimation of oceanic precipitation efficiency in cloud models. *J Atmos Sci*. <https://doi.org/10.1175/JAS3587.1>
- Tinel C, Testud J, Hogan RJ, Protat A, Delanoe J, Bouniol D (2005) The retrieval of ice cloud properties from cloud radar and lidar synergy. *J Appl Meteorol*. <https://doi.org/10.1175/JAM2229.1>
- Vivekanandan J, Martner B, Politovich MK, Zhang G (1999) Retrieval of atmospheric liquid and ice characteristics using dual-wavelength radar observations. *IEEE Trans Geosci Remote Sens*. <https://doi.org/10.1109/36.789629>
- Vivekanandan J, Zhang G, Politovich MK (2001) An assessment of droplet size and liquid water content derived from dual-wavelength radar measurements to the application of aircraft icing detection. *J Atmos Ocean Technol*. [https://doi.org/10.1175/1520-0426\(2001\)018%3c1787:AAODSA%3e2.0.CO;2](https://doi.org/10.1175/1520-0426(2001)018%3c1787:AAODSA%3e2.0.CO;2)
- Wang Z, Sassen K (2001) Cloud type and property retrieval using multiple remote sensors. *J Appl Meteorol*. [https://doi.org/10.1175/1520-0450\(2001\)040%3c1665:CTAMP%3e2.0.CO;2](https://doi.org/10.1175/1520-0450(2001)040%3c1665:CTAMP%3e2.0.CO;2)
- Webster PJ, Magana VO, Palmer TN, Shukla J, Tomas RA, Yanai MU, Yasunari T (1998) Monsoons: processes predictability and the prospects for prediction. *J Geophys Res Ocean*. <https://doi.org/10.1029/97JC02719>
- Wood N (2008) Level 2B radar-visible optical depth cloud water content (2B-CWC-RVOD) process description document. Version 5 1-26

**Publisher's Note** Springer Nature remains neutral with regard to jurisdictional claims in published maps and institutional affiliations.